AIP | Journal of Renewable and Sustainable Energy

Control methods of the switched reluctance motor in electric vehicle during acceleration

Fathy El Sayed Abdel-Kader, M. Z. Elsherif, Naser M. B. Abdel-Rahim, and Mohamed M. Fathy

Citation: J. Renewable Sustainable Energy **4**, 063142 (2012); doi: 10.1063/1.4772964
View online: http://dx.doi.org/10.1063/1.4772964
View Table of Contents: http://jrse.aip.org/resource/1/JRSEBH/v4/i6
Published by the American Institute of Physics.

Control methods of the switched reluctance motor in electric vehicle during acceleration

Fathy El Sayed Abdel-Kader,[1,a)] M. Z. Elsherif,[2,b)]
Naser M. B. Abdel-Rahim,[2,c)] and Mohamed M. Fathy[2,d)]
[1]*Faculty of Engineering, Menofia University, G. A. Nasser St., Shibin El kom, Egypt*
[2]*Faculty of Engineering, Benha University, 108, Shoubra St., Cairo, Egypt*

(Received 29 July 2012; accepted 30 November 2012; published online 20 December 2012)

In this paper, the equations describing the performance of the electric vehicle are derived. Performance characteristics for each part in the vehicle system are obtained when the vehicle is accelerated under voltage, turn on, and turn off angle control. A comparison between the different methods of control is established. From these comparisons, it can be noticed that the acceleration time, for the case at which the turn on angle is controlled, will be smaller than that for the other cases; also the motor efficiency, at the voltage control method, has the highest value especially at the higher values of the vehicle speed. © *2012 American Institute of Physics*. [http://dx.doi.org/10.1063/1.4772964]

I. INTRODUCTION

At present, the internal combustion engine (ICE) vehicle is a major source of urban pollution. According to the figures published by the U.S. Environmental Protection Agency (EPA), conventional ICE automobiles currently contribute by 40%–50% of ozone (nonmethane organic gases NMOG), 80%–90% of carbon monoxide (CO), and 50%–60% of air toxins (nitrogen oxides NOx) found in urban areas. The other main objection regarding ICE vehicles, beside air pollution, is their extremely low efficiency use of fossil fuel. Hence, the problem related to the ICE vehicles is threefold: environmental, economical, as well as political. These concerns have forced all governments around the world to consider alternative vehicle concepts.[1–3]

Electric vehicles (EVs) present the most promising solutions for reducing vehicular emissions. EVs represent the only commonly known group of vehicles that qualified as zero emission vehicles (ZEVs). These vehicles use electric motors for the propulsion system and batteries as electrical energy storage devices.[1,2] Figure 1 shows the Drivetrain of the electric vehicle.

Switched reluctance motor (SRM) is surely the simplest of electrical machines. They consist of a stator having the excitation windings and a magnetic rotor with saliency. Rotor conductors are not required because torque is produced by the tendency of the rotor to align with the stator poles, producing the flux wave in order to maximize the stator flux linkages that result from a given applied phase current.

Due to the simple and rugged motor construction, lower weight, potentially lower production cost, inherent fault tolerance, undemanding cooling, high operating efficiency, high torque density, and excellent torque–speed characteristics, the SRM drives are considered the attractive solution for EV applications.[4–15] Traction performances of EV applications depend on the performance characteristics of SRM drives. Thus, the excellent motoring operation of the SRMs is the important factor for EVs with high performances.

[a)]E-mail: fatkader2@yahoo.com.
[b)]E-mail: elsherif.mohsen@yahoo.com.
[c)]E-mail: nabdelrahim@gmail.com.
[d)]Author to whom correspondence should be addressed. Electronic mail: eng_mohfathysaad@yahoo.com. Tel.: 01226283560. Fax: +(202) 26708584.

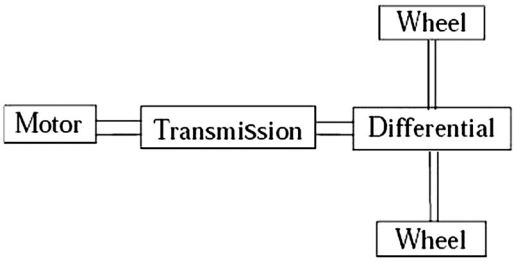

FIG. 1. The EV Drivetrain.

II. PERFORMANCE EQUATIONS OF THE EV WITH ACCELERATION MODE

To investigate the EV performance at acceleration, it will be assumed that the vehicle is accelerated under certain values of the motor terminal voltage, turn on, and turn off angles.

The voltage equation of each phase winding can be expressed as[16]

$$v = i\mathrm{R} + \frac{\mathrm{d}\lambda\,(i,\theta)}{\mathrm{dt}}. \tag{1}$$

Neglecting the saturation of the magnetic circuit, the phase flux linkage can be expressed by

$$\lambda(i,\theta) = \mathrm{L}(\theta)i, \tag{2}$$

By substituting Eq. (2) into Eq. (1), the motor phase voltage can be written as

$$v = i\mathrm{R} + \mathrm{L}(\theta)\frac{\mathrm{d}i}{\mathrm{dt}} + i\frac{\mathrm{dL}(\theta)}{\mathrm{dt}}. \tag{3}$$

Also, Eq. (3) can be rewritten as

$$v = i\mathrm{R} + \mathrm{L}(\theta)\frac{\mathrm{d}i}{\mathrm{d}\theta}\frac{\mathrm{d}\theta}{\mathrm{dt}} + i\frac{\mathrm{dL}(\theta)}{\mathrm{d}\theta}\frac{\mathrm{d}\theta}{\mathrm{dt}}. \tag{4}$$

At steady state, the motor speed can be determined as a function of the rotor position by

$$\omega = \frac{\mathrm{d}\theta}{\mathrm{dt}}, \tag{5}$$

where ω and θ are the motor speed in elec. rad/s and the rotor position in elec. rad, respectively.

Substituting Eq. (5) into Eq. (4), the motor phase voltage can be expressed as

$$v = i\mathrm{R} + \mathrm{L}(\theta)\,\omega\frac{\mathrm{d}i}{\mathrm{d}\theta} + i\omega\frac{\mathrm{dL}(\theta)}{\mathrm{d}\theta}, \tag{6}$$

where the three terms of the above equation represent the resistive drop, the self, and rotational EMF, respectively.

Finally, after rearranging Eq. (6), the motor phase voltage can be rewritten as

$$v = \left(\mathrm{R} + \omega\frac{\mathrm{dL}(\theta)}{\mathrm{d}\theta}\right)i + \omega\,\mathrm{L}(\theta)\frac{\mathrm{d}i}{\mathrm{d}\theta}. \tag{7}$$

From Figure 2, the motor phase inductance can be represented as a function of the rotor position as

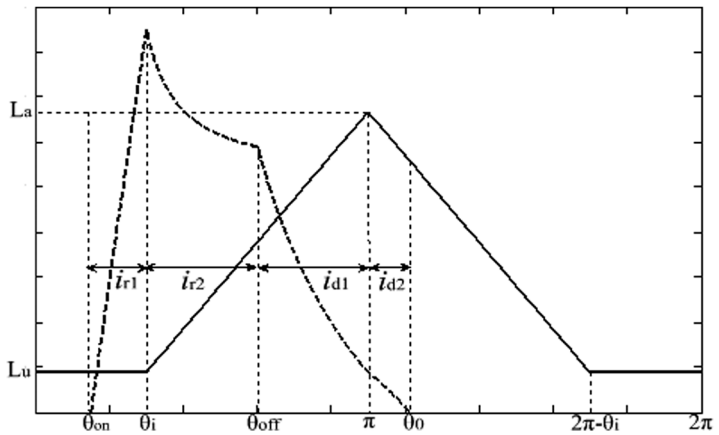

FIG. 2. Motor phase inductance and current against the rotor position.

$$\begin{aligned} L(\theta) &= L_u && 0 \le \theta \le \theta_i, \\ L(\theta) &= k_1\theta - k_2 && \theta_i \le \theta \le \pi, \\ L(\theta) &= -k_1\theta - k_3 && \pi \le \theta \le (2\pi - \theta_i), \\ L(\theta) &= L_u && (2\pi - \theta_i) \le \theta \le 2\pi. \end{aligned} \tag{8}$$

The constants k_1, k_2, k_3 and θ_i are equal

$$\begin{aligned} k_1 &= \frac{L_a - L_u}{\pi - \theta_i}, \\ k_2 &= \frac{L_a\theta_i - L_u\pi}{\pi - \theta_i}, \\ k_3 &= \frac{-\pi\,(L_a - L_u) - L_a(\pi - \theta_i)}{\pi - \theta_i}, \\ \theta_i &= \pi - N_r\beta_r. \end{aligned}$$

According to the motor phase voltage, there are two modes of operation of the SRM. At the first mode of operation, the motor phase voltage is connected to the DC supply voltage Vs, thus the motor phase current will be increased. At the second mode, the applied voltage on the motor phase is the negative value of the DC supply voltage, thus the motor phase current will be decayed to zero value.

Substituting Eq. (8) into Eq. (7) taking into account the specified modes of operation, the motor phase current can be obtained for each rotor position range, included in Figure 2, as

$$\begin{aligned} i_{r1}(\theta) &= \frac{V_s}{R}\left[1 - e^{-(\theta - \theta_{on})R/(\omega L_u)}\right]_{\theta_{on} \le \theta \le \theta_i}, \\ i_{r2}(\theta) &= \frac{V_s}{R + k_1\omega} + \left[i_{r1}(\theta_i) - \frac{V_s}{R + k_1\omega}\right]\left[\frac{k_1\theta_i - k_2}{k_1\theta - k_2}\right]^{\left[\frac{R + k_1\omega}{k_1\omega}\right]}_{\theta_i \le \theta \le \theta_{off}}, \\ i_{d1}(\theta) &= \frac{-V_s}{R + k_1\omega} + \left[i_{r2}(\theta_{off}) + \frac{V_s}{R + k_1\omega}\right]\left[\frac{k_1\theta_{off} - k_2}{k_1\theta - k_2}\right]^{\left[\frac{R + k_1\omega}{k_1\omega}\right]}_{\theta_{off} \le \theta \le \pi}, \\ i_{d2}(\theta) &= \frac{-V_s}{R - k_1\omega} + \left[i_{d1}(\pi) + \frac{V_s}{R - k_1\omega}\right]\left[\frac{-k_1\pi - k_3}{-k_1\theta - k_3}\right]^{\left[\frac{R - k_1\omega}{-k_1\omega}\right]}_{\pi \le \theta \le \theta_0}, \end{aligned} \tag{9}$$

where these equations are derived to represent the following range for the turn on and turn off angles: $\theta_{on} < \theta_i$ and $\theta_{off} < \pi$.

Also θ_0 is the angle at which the motor phase current equals zero after decaying. This angle can be determined from Eq. (9) by putting ($i_{d2} = 0$ and $\theta = \theta_0$)

$$\theta_0 = \frac{1}{L_a - L_u}\left[\frac{-L_a(\pi - \theta_i)[(R - k_1\omega)i_{d1}(\pi) + V_s]^{k_4}}{V_s^{k_4}} + \pi(L_a - L_u) + L_a(\pi - \theta_i)\right], \tag{10}$$

where the constant k_4 is equal

$$k_4 = \frac{-k_1\omega}{R - k_1\omega}.$$

Therefore, the motor torque is expressed by

$$T_e = \frac{1}{2}i^2\frac{dL(\theta)}{d\theta}. \tag{11}$$

The motor speed can be expressed in terms of the vehicle speed as

$$\omega_m = m\frac{V_{veh}}{r_{wh}}, \tag{12}$$

where m is the gear ratio of the mechanical coupling between the motor and the axle of the vehicle wheels.

Assuming lossless transmission, the developed torque at the shaft of the wheel axle can be determined by

$$T_{d\_wh} = m\,T_e. \tag{13}$$

The corresponding tractive force will, thus, be

$$F_{TR} = \frac{T_{d\_wh}}{r_{wh}}. \tag{14}$$

The tractive force developed at the shaft of the wheel axle during acceleration can be expressed by

$$F_{TR} = k_m M_{veh}\frac{dV_{veh}}{dt} + F_{RL}, \tag{15}$$

where the road load force is[1,6,10–13]

$$F_{RL} = Co\,M_{veh}g + M_{veh}g\sin(\beta) + 0.5\,\rho\,C_D\,A_F V_{veh}{}^2. \tag{16}$$

Thus, the load torque at the shaft of the wheel axle can be expressed by

$$T_{wh} = F_{RL}\,r_{wh} + T_b. \tag{17}$$

Also, the load torque at the shaft of the motor axle can be expressed by

$$T_L = \frac{T_{wh}}{m}. \tag{18}$$

Therefore, from Eq. (15), the acceleration of the vehicle can be expressed by[4]

$$\frac{dV_{veh}}{dt} = \frac{1}{k_m M_{veh}}(F_{TR} - F_{RL}). \tag{19}$$

Also using the motor torque and speed, the motor output power can be expressed by

$$P_{mo} = T_e\, \omega_m. \tag{20}$$

The motor power losses can be determined by

$$P_{Loss} = n_{ph}\, I_{ph}{}^2\, R, \tag{21}$$

where I_{ph} is the average value of the motor phase current.

The motor excessive energy can be determined from

$$E_{exc} = n_{ph}(I_{ph} - I_r)^2\, R\, dt, \tag{22}$$

where I_r and dt are the rated value of the motor phase current and the time step.

III. PRINCIPLE OF NUMERICAL SOLUTION

Starting from zero vehicle speed at certain values of the motor turn on, turn off angles, and terminal voltage, from Eq. (12), the motor speed would be equal to zero. From Eqs. (9) and (10), the motor phase current can be determined. When the motor phase current exceed the rated value, the motor voltage, turn on, or turn off angles are controlled to make the motor phase current within permissible value.

Then using the phase current into Eq. (11), the motor developed torque, T_e, can be obtained. Also from Eqs. (20) and (21), the motor output power, P_{mo}, and the motor power losses, P_{Loss}, can be determined, respectively. Multiplying the predetermined motor phase current by the motor terminal voltage, the motor input power, P_{m_in}, can also be obtained. Thus, using the motor input and output power, the motor efficiency, η_m, can be obtained. Using Eq. (22), the motor excessive energy, E_{exc}, can be determined and then from Eq. (6), the motor rotational and self EMF can be calculated. From Eqs. (14) and (16), the tractive and road load forces can be determined at this vehicle speed, respectively.

Using these values of the tractive and road load force into Eq. (19), the next vehicle speed can be obtained by integrating this equation numerically over an appropriate time step. For the second and following time steps of numerical solution, the corresponding motor speed is obtained from Eq. (12). Then Eq. (11) is used to obtain its motor developed torque, and the corresponding tractive force is obtained from Eq. (14). This process continues until the vehicle reaches steady-state speed.

IV. SIMULATION RESULTS AT THE DIFFERENT METHODS OF CONTROL

The approach presented in Eq. (3) was applied using 4th order Runge-Kutta numerical method of integration. Using the data of the switched reluctance motor and vehicle given in Appendix, the performance characteristics of the vehicle are obtained when the vehicle is accelerated to 160 km/h under three methods of control. At the first method of control, the vehicle is accelerated under a controlled terminal voltage, to maintain the phase current within the rated condition, while the turn on and turn off angles are maintained at the optimum values (0°, 30°, respectively). At the second method of control, the vehicle is accelerated under controlled turn on angle, to maintain the phase current within the rated condition, while the motor terminal voltage and turn off angle are maintained constant at the optimum values (280 V, 30°, respectively). At the third method of control, the vehicle is accelerated under controlled turn off angle, to maintain the phase current within the rated condition, while the motor terminal voltage and turn on angle are maintained constant at the optimum values (280 V, 0°, respectively).

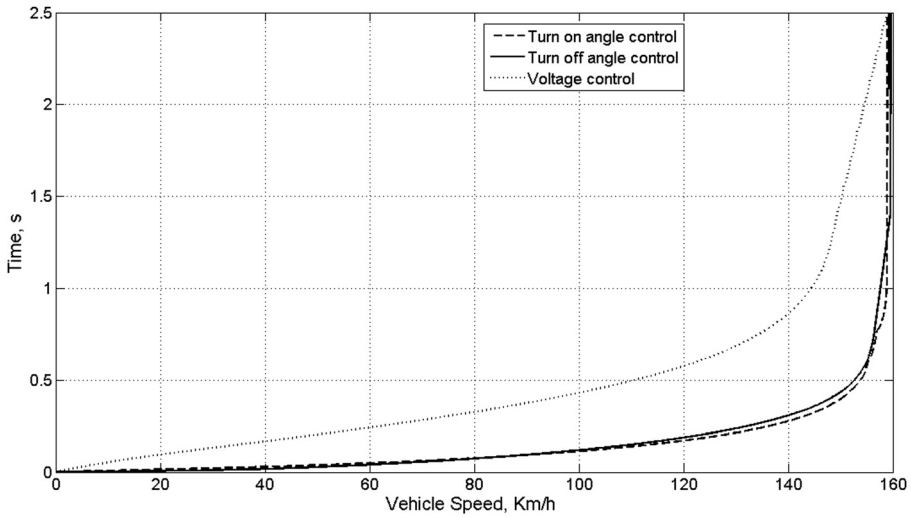

FIG. 3. Time versus vehicle speed at vehicle acceleration under the different control methods.

Figure 3 shows the variation of the vehicle speed throughout the acceleration period in the three cases when the vehicle is accelerated under voltage control (at $\theta_{on} = 0^\circ$ and $\theta_{off} = 30^\circ$), turn on angle control (where $V_s = 280\,V$ and $\theta_{off} = 30^\circ$), and when the vehicle is accelerated under the turn off angle control (where $V_s = 280\,V$ and $\theta_{on} = 0^\circ$). From this figure, it is clear that in the three cases the vehicle will reach to the same final steady-state speed (160 km/h) and the acceleration time, for the case at which the turn on angle is controlled, will be smaller than that for the other cases; also the acceleration time, for the case of voltage control, will be the largest.

Also, Figures 4–6 show the motor terminal voltage, turn on, and turn off angles, respectively, when the vehicle is accelerated under different methods of control illustrated previously. From Figure 4, it is clear that the motor terminal voltage will be varied from 50 V to 280 V, during acceleration under the voltage control, but in the other cases, the motor terminal voltage is maintained constant at the optimum value (280 V). Also from Figure 5, it is noticed that the motor turn on angle started from 17.5° to 0°, during acceleration under the turn on angle control, while in the other cases, the turn on angle will be maintained constant at the optimum

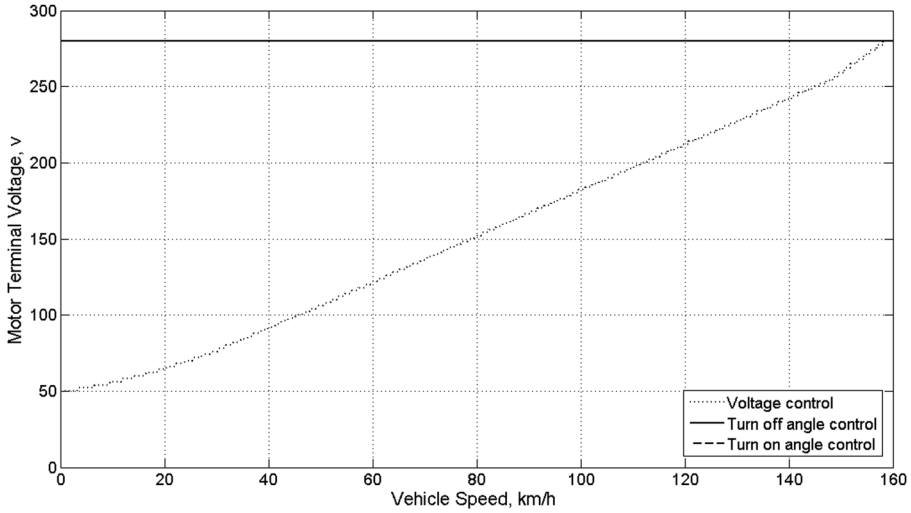

FIG. 4. Motor terminal voltage versus vehicle speed at acceleration under the different control methods.

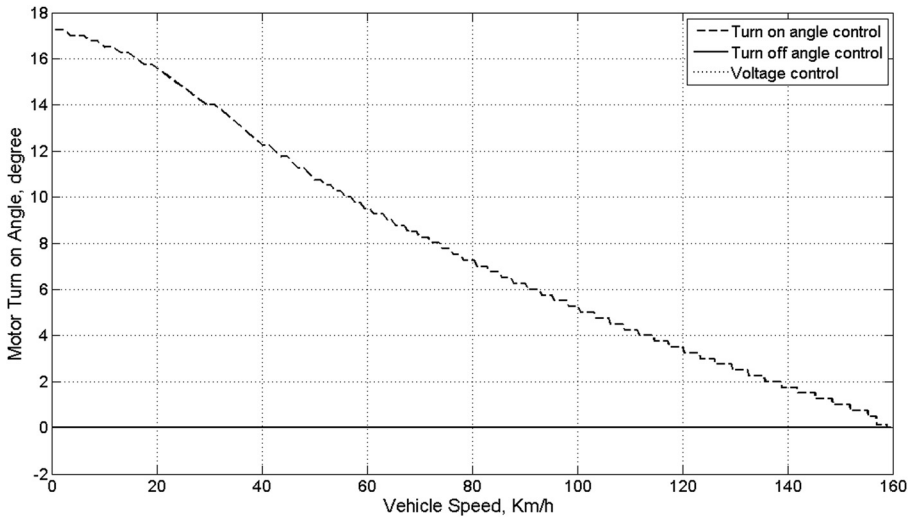

FIG. 5. Motor turn on angle versus vehicle speed at acceleration under the different control methods.

value (0°). Finally from Figure 6, it is clear that the motor turn off angle will be varied from 14° to 30°, during acceleration under the turn off angle control, but in the other cases, the turn off angle is maintained constant at the optimum value (30°).

Using the values of the vehicle speed, which are obtained, into Eqs. (9) and (10), the motor phase current can be plotted against vehicle speed, for the different cases of control illustrated previously, as shown in Figure 7. From this figure, it is noticed that the motor phase current is maintained constant within the rated condition during the acceleration period under the different cases of control.

Using the values of the vehicle speed, which are obtained previously, into Eqs. (9) and (10) then substituting into Eq. (11), the characteristics of the motor developed torque, T_e, can be obtained for the different methods of control illustrated earlier. Also from Eq. (18), the motor load torque, T_L, can be estimated. Then the motor developed torque and load torque are drawn versus the vehicle speed, during acceleration until steady-state conditions are reached, as shown in Figure 8. From this figure, it is clear that the motor developed torque, for the case of

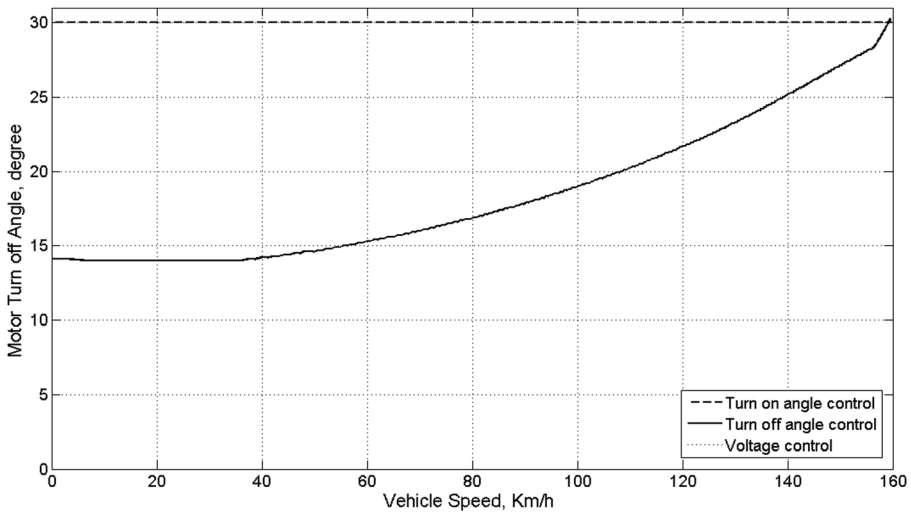

FIG. 6. Motor turn off angle versus vehicle speed at acceleration under the different control methods.

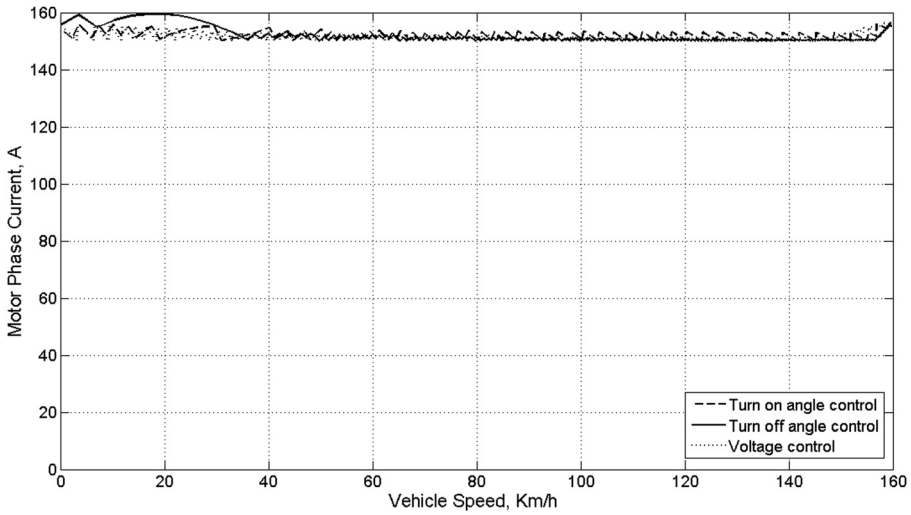

FIG. 7. Motor phase current versus vehicle speed at acceleration under the different control methods.

voltage control, increases slightly as the vehicle accelerates, but for the other cases of control, the motor developed torque started high and then decrease as the vehicle speed increases. At certain vehicle speed, the motor developed torque, at the voltage control method, has lower values than that of the other methods of control during the acceleration period. Also the motor developed torque, at the turn off angle control method, has the highest value especially at the lower vehicle speed (<40 km/h), and the motor developed torque, at the turn on angle control method, has the highest value at vehicle speed higher than 40 km/h. Finally, the load torque increases as the vehicle speed increases up to steady-state speed at which the curves of the developed and load torques are intersected.

Using the motor developed torque, calculated from Eq. (11), and the motor speed, calculated from Eq. (12), into Eq. (20), the characteristics of the motor output power, P_{mo}, can be obtained and plotted against the vehicle speed, for the three cases of control illustrated earlier, as shown in Figure 9. From this figure, it is noticed that the motor output power, for the case of turn off angle control, decreases as the vehicle accelerates, up to 40 km/h, and then the power increases as the vehicle speed increases, but for the other cases of control, the motor

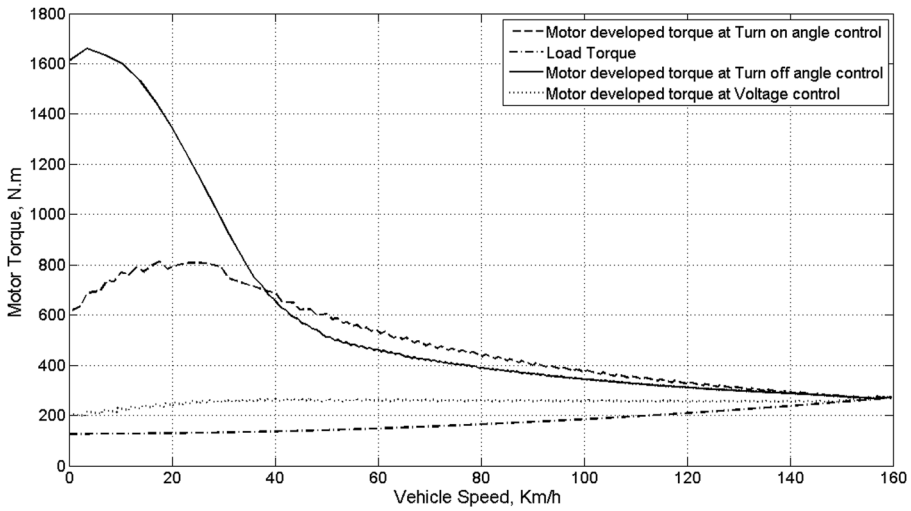

FIG. 8. Motor developed torque and load torque versus vehicle speed at acceleration under the different control methods.

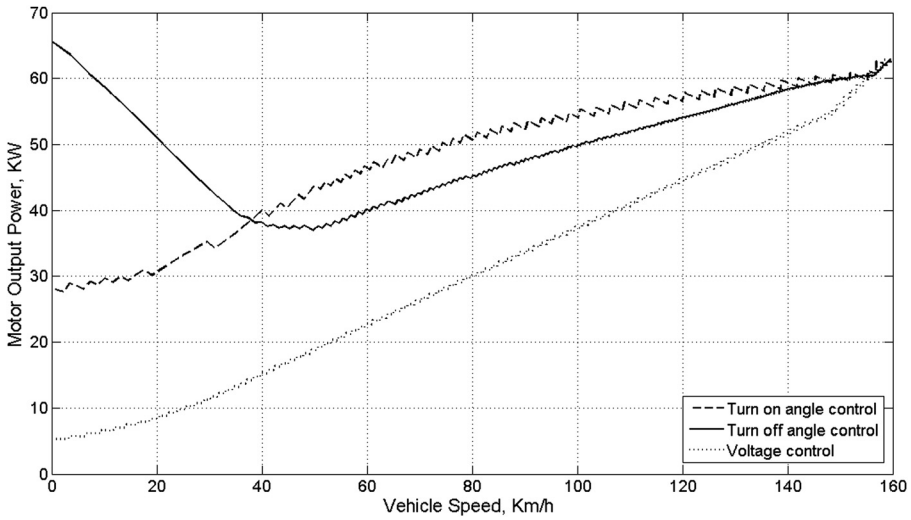

FIG. 9. Motor output power versus vehicle speed at acceleration under the different control methods.

output power increases as the vehicle accelerates up to the final steady-state speed. At certain vehicle speed, the motor output power, at the voltage control method, has the lower values than that of the other methods of control. Also the motor output power, at the turn off angle control method, has the highest values at the lower vehicle speed (<40 km/h) and the motor output power, at the turn on angle control method, has the highest values at the other values of vehicle speed.

Using the values of the motor phase current, which are obtained into Eq. (21), the motor power losses, P_{Loss}, can be drawn versus the vehicle speed, during acceleration until steady-state conditions are reached, as shown in Figure 10. From this figure, it is clear that the motor power losses, for the different methods of control, are maintained constant, due to the constancy of the phase current, as the vehicle accelerates up to the final steady-state speed.

Using the predetermined motor phase current into Eq. (22), the motor excessive energy, E_{exc}, can be computed and plotted as shown in Figure 11. From this figure, it is clear that at certain vehicle speed, the motor excessive energy, at the turn off angle control method, has higher values than that of the other control methods during the vehicle acceleration. Also the

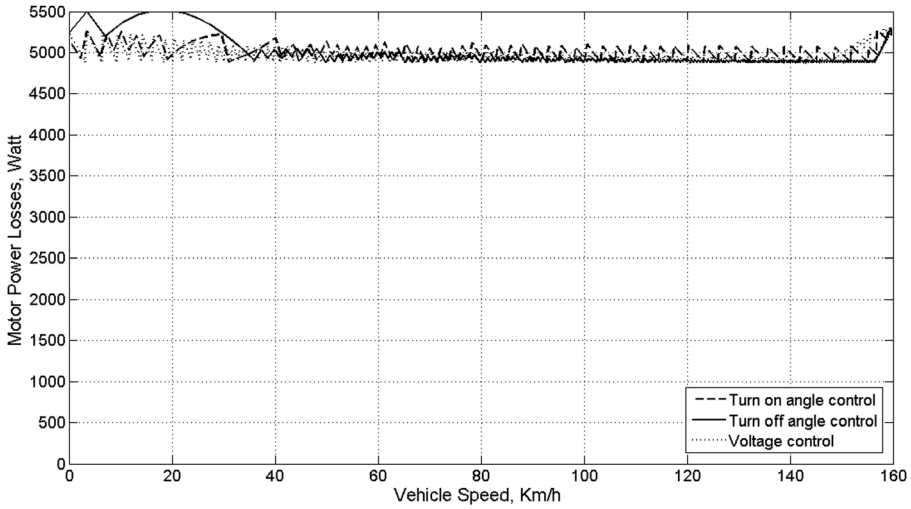

FIG. 10. Motor power losses versus vehicle speed at acceleration under the different control methods.

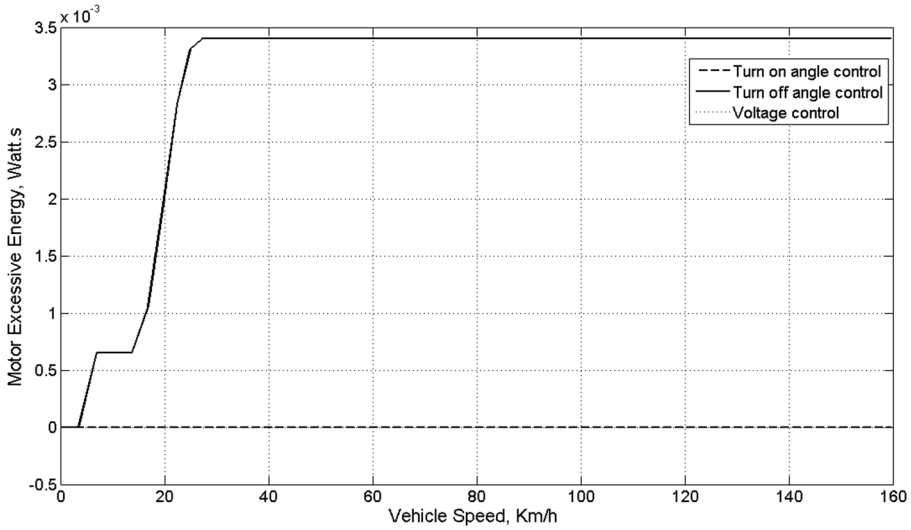

FIG. 11. Motor excessive energy versus vehicle speed at acceleration under the different control methods.

values of the motor excessive energy, for the different methods of control, are very small thus it can be neglected.

Multiplying the predetermined motor phase current which is obtained at the two cases illustrated earlier, from Eqs. (9) and (10), by the motor terminal voltage, the motor input power, P_{m_in}, can be also computed and plotted as shown in Figure 12. From this figure, it is noticed that, for the case of turn off angle control, the motor input power has a higher value and then decrease as the vehicle speed increases and for the other cases of control, the motor input power will increase as the vehicle accelerates up to the final steady-state speed at which the curves are intersected. At certain vehicle speed, the motor input power, at the case of turn off angle control, has the highest values; on the contrary, the motor input power will have the lowest values at the voltage control method.

Using the values of the motor input power and the motor output power which are obtained previously, the characteristics of the motor efficiency, $\eta_{m,}$ can be obtained against the vehicle speed as shown in Figure 13. From this figure, it is clear that, for the different methods of

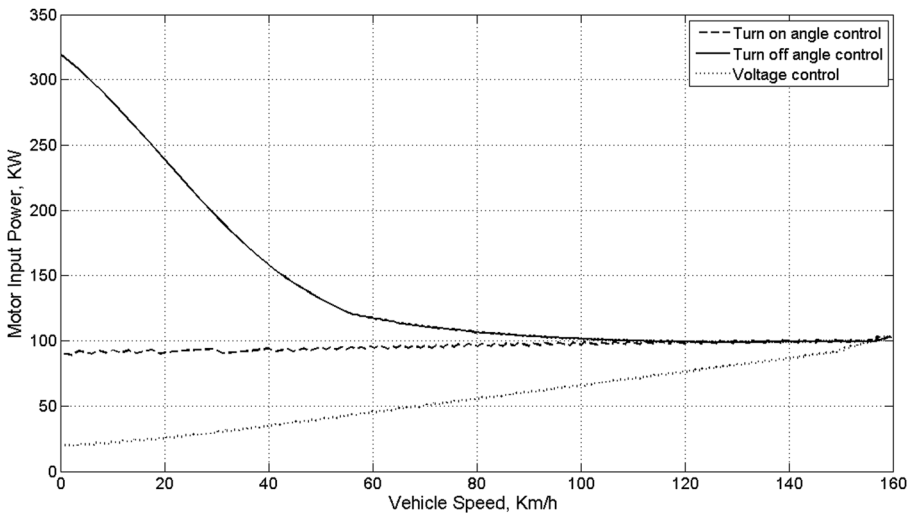

FIG. 12. Motor input power versus vehicle speed at acceleration under the different control methods.

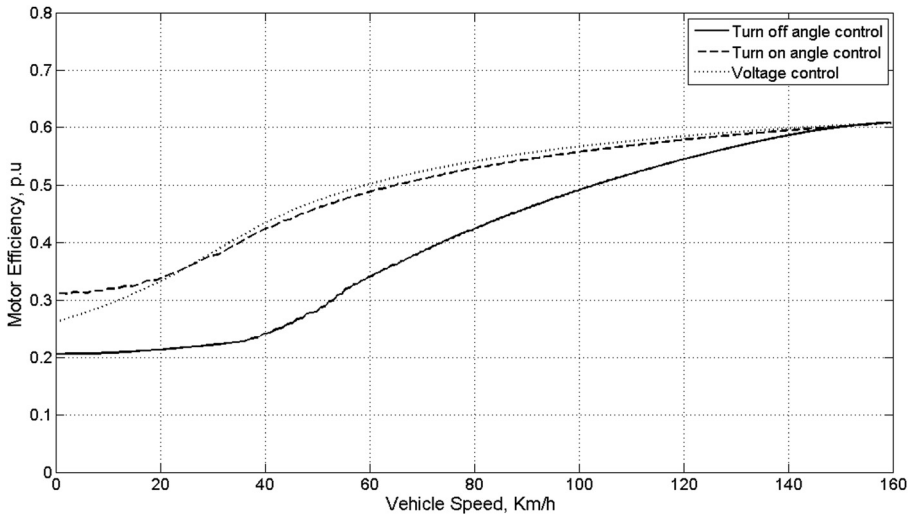

FIG. 13. Motor efficiency versus vehicle speed at acceleration under the different control methods.

control, the motor efficiency increases as the vehicle speed increases. At certain vehicle speed, the motor efficiency, at the voltage control method, has the highest value especially at any vehicle speed higher than 25 km/h, and the motor efficiency, at the turn on angle control method, will have the largest value at other values of vehicle speed. But the motor efficiency at the case of turn off angle control always has the lower value during the acceleration period. Also the motor efficiency, at the voltage control method, has the highest value especially at any vehicle speed higher than 25 km/h and the motor efficiency, at the turn on angle control method, will have the largest value at other values of vehicle speed. But the motor efficiency at the case of turn off angle control always has the lower value during the acceleration period.

From Eq. (6), the motor rotational and self EMF can be calculated for the different cases of control illustrated previously. Then the rotational and self EMF are plotted versus vehicle speed as shown in Figures 14 and 15, respectively.

From Figure 14, it is clear that the motor rotational EMF increases as the vehicle speed increases for all the cases of control. Then at a certain vehicle speed, the rotational EMF will

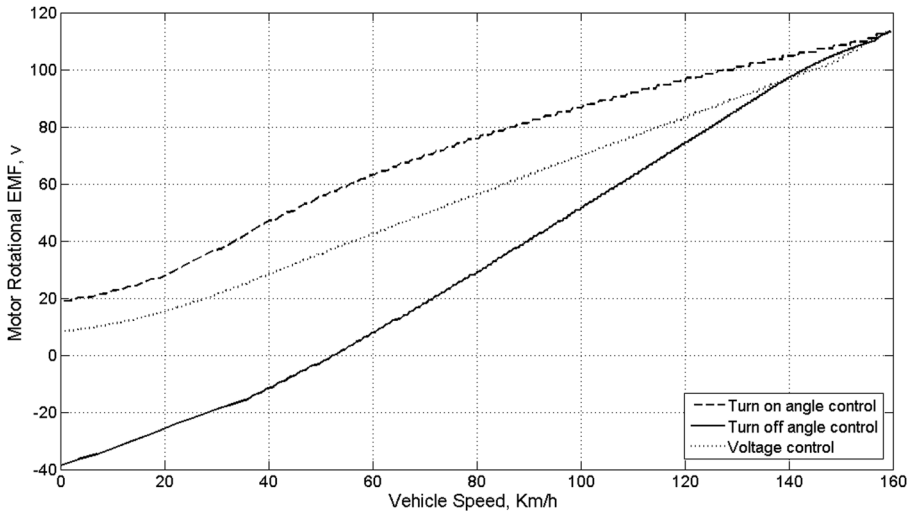

FIG. 14. Motor rotational EMF versus vehicle speed at acceleration under the different control methods.

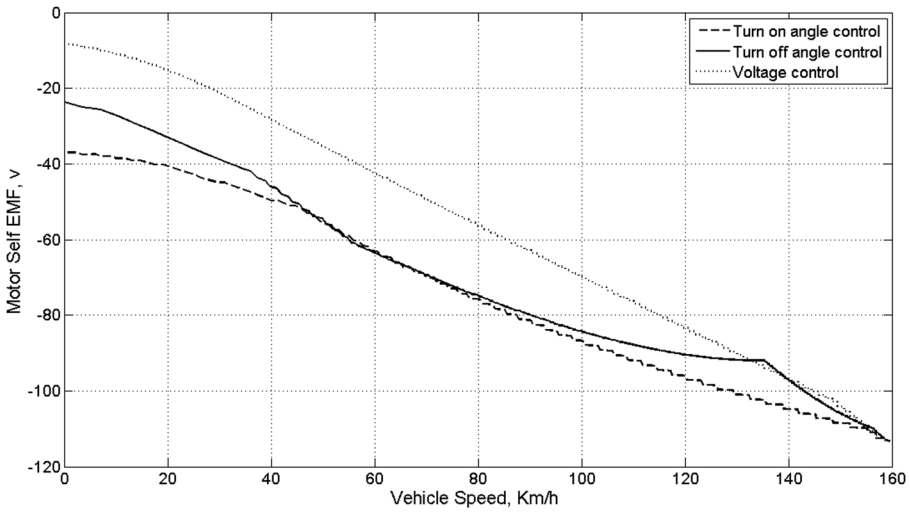

FIG. 15. Motor self EMF versus vehicle speed at acceleration under the different control methods.

have the larger values for the case of turn on angle control; on contrary, the rotational EMF will have the lower values for the case of turn off angle control especially at vehicle speed lower than 140 km/h. Also from Figure 15, it is noticed that the motor self EMF, for the different cases of control, decreases as the vehicle accelerates up to the final steady-state speed. At a certain vehicle speed, the self EMF will have the higher values at the case of voltage control; on contrary, the self EMF will have the lower values for the case of turn on angle control.

V. CONCLUSIONS

From the performance characteristics of the EV operating in the acceleration mode under the different methods of control, it can be noticed that the acceleration time, for the case at which the turn on angle is controlled, will be smaller than that for the other cases; also the acceleration time, for the case of voltage control, will be the largest.

Also the motor efficiency, at the voltage control method, has the highest value especially at any vehicle speed higher than 25 km/h and the motor efficiency, at the turn on angle control method, will have the largest value at other values of vehicle speed. But the motor efficiency at the case of turn off angle control always has the lower value during the acceleration period.

NOMENCLATURE

A_f	Equivalent frontal area of the vehicle in m^2
C_0	Coefficient of rolling resistance
C_D	Aerodynamic drag coefficient
E_{exc}	Motor excessive energy
F_{RL}	Road load force in N
F_{TR}	Tractive force in N
g	Gravitational acceleration constant in m/s^2
i	Motor phase current
I_{ph}	The average value of the motor phase current in A
I_r	Rated value of the motor phase current in A
$k_{1\ldots}$ K_4	Constants
k_m	Rotational inertia coefficient
L	Motor phase inductance
L_a	Aligned inductance in mH
L_u	Unaligned inductance in mH

m	The gear ratio of the mechanical coupling between the motor and the axle of the vehicle wheels
M_{veh}	Total mass of the vehicle in kg
n_{ph}	Number of motor phases
N_r	Number of rotor poles
P_{Loss}	Motor power losses in W
$P_{m\text{-}in}$	Motor input power in W
P_{mo}	Motor output power in W
R	Motor phase resistance in Ω
r_{wh}	Radius of the wheel in m
T_b	Frictional brake torque in Nm
T_{d_wh}	The developed torque at the shaft of the wheel axle
T_e	Motor developed torque in Nm
T_L	Load torque at the shaft of the motor axle in Nm
T_{wh}	Load torque at the shaft of the wheel axle in Nm
v	Motor phase voltage in V
V_s	DC supply voltage in V
V_{veh}	Vehicle speed in km/h
β	Road grade angle
β_r	Rotor poles arc
θ	Rotor position in elec. rad
θ_0	The angle at which the motor phase current equal zero after decaying
θ_{off}	Turn off angle
θ_{on}	Turn on angle
λ	Motor phase flux linkage
ρ	Air density in kg/m^3
ω	Motor speed in elec. rad/s
ω_m	Motor speed in rad/s

APPENDIX: DATA OF THE SRM AND EV

Data of the SRM: $P_r = 60$ kW, $V_r = 280$ V, $R = 0.072$ Ω, $L_a = 3.334$ mH, $L_u = 0.445$ mH, $Nr = 4$, $Ns = 6$, $n_{ph} = 3$, $Bs = Br = \pi/6$, $j = 0.3$, $b = 0.0183$, $n_r = 2214$ rpm.

Vehicle dynamic parameters: $\rho = 1.225$ kg/m^3, $C_D = 0.3$, $A_f = 2$ m^2, $M_{veh} = 1500$ kg, $r_{wh} = 0.2794$ m, $Tb = 0$, $V_{veh\text{-}max} = 160$ km/h, $V_f = 100$ km/h, $km = 1.08$, $C_0 = 0.01$, $g = 9.81$ m/s^2, $m = 1.4575$, $\beta = 2°$, $\eta_{tmw} = 1.00$.

[1]M. Ehsani, K. M. Rahman, and H. A. Toliyat, "Propulsion system design of electric and hybrid vehicles," IEEE Trans. Ind. Electron. **44**(1), 19–27 (1997).
[2]I. Husain, *Electric and Hybrid Vehicles Design Fundamentals* (Taylor & Francis e-Library, 2005).
[3]M. Ehsani, Y. Gao, S. E. Gay, and A. Emadi, *Modern Electric, Hybrid Electric, and Fuel Cell Vehicles Fundamentals, Theory, and Design* (CRC, 2005).
[4]I. Husain and M. S. Islam, "Design, modeling and simulation of an electric vehicle system," in *Society of Automotive Engineers (SAE), International Congress and Exposition, Detroit, Michigon, March 1–4, 1995* (Society of Automotive Engineers (SAE), 1999), pp. 1–9.
[5]K. M. Rahman, B. Fahimi, G. Suresh, A. Velayutham Rajarathnam, and M. Ehsani, "Advantages of switched reluctance motor applications to EV and HEV: Design and control issues," IEEE Trans. Ind. Appl. **36**(1), 111–121 (2000).
[6]S. Sadeghi, J. Milimonfared, and M. Mirsalim, "Dynamic modeling and simulation of a series hybrid electric vehicle using a switched reluctance motor," in Proceeding of International Conference on Electrical Machines and Systems, Seoul, Korea, October 8–11, 2007.
[7]S. Kachapornkul, P. Jitkreeyarn, P. Somsiri, and K. Tungpimolrut, "A design of 15 kW switched reluctance motor for electric vehicle applications," in *Proceeding of International Conference on Electrical Machines and Systems* (Institute of Electrical and Electronics Engineers (IEEE), Seoul, Korea, 2007), pp. 1690–1693.
[8]M. A. Cinar and F. Erfan Kuyumcu, "Design and drives simulation of an in-wheel switched reluctance motor for electric vehicle applications," in *IEEE International Electric Machines & Drives Conference (IEMDC '07)* (Institute of Electrical and Electronics Engineers (IEEE), Antalya, Turkey, 2007), pp. 50–54.
[9]S. Cui, Y. Yuan, and T. Wang, "Research on switched reluctance double-rotor motor used for hybrid electric vehicle," in *IEEE International Conference on Electrical Machines and Systems (ICEMS)* (Institute of Electrical and Electronics Engineers (IEEE), Wuhan, China, 2008), pp. 3393–3396.

[10]S. Aida, A. Komatsuzaki, and I. Miki, "Basic characteristics of electric vehicle using 40 kW switched reluctance motor," in *IEEE International Conference on Electrical Machines and Systems (ICEMS)* (Institute of Electrical and Electronics Engineers (IEEE), Wuhan, China, 2008), pp. 3358–3361.
[11]X. D. Xue, J. K. Lin, Z. Zhang, T. W. Ng, K. F. Luk, K. W. E. Cheng, and N. C. Cheung, "Study of motoring operation of in-wheel switched reluctance motor drives for electric vehicles," in *3rd IEEE International Conference on Power Electronics Systems and Applications (PESA)* (Institute of Electrical and Electronics Engineers (IEEE), Hong Kong, 2009), pp. 1–6.
[12]J. Lin, K. W. Eric Cheng, Z. Zhang, and X. Xue, "Experimental investigation of in-wheel switched reluctance motor driving system for future electric vehicles," in *IEEE 3rd International Conference on Power Electronics Systems and Applications (PESA)* (Institute of Electrical and Electronics Engineers (IEEE), Hong Kong, 2009), pp. 1–6.
[13]X. D. Xue, K. W. E. Cheng, T. W. Ng, and N. C. Cheung, "Multi-objective optimization design of in-wheel switched reluctance motors in electric vehicles," IEEE Trans. Ind. Electron. **57**(9), 2980–2987 (2010).
[14]E. El-Kharashi and H. M. Hassanien, "Reconstruction of the switched reluctance motor stator," J. Electr. Eng. **63**(1), 3–12 (2012).
[15]V. Prakash Kumar, S. Prabhu, V. Saravanan, V. Chandrasekar, R. Arumugan, and M. Arumugam, "Vibration reduction of switched reluctance hub motor," in International Conference on Computing and Control Engineering (ICCCE 2012), Chennai, India, April 12 and 13, 2012.
[16]S. Pratapgiri and P. Polaki Venkata Narsimha, "Direct torque control of 4 phase 8/6 switched reluctance motor drive for constant torque load," World J. Model. Simul. **8**(3), 185–195 (2012).